Reaction analogy based forcing for incompressible scalar turbulence

Don Daniel,[1] Daniel Livescu,[1,*] and Jaiyoung Ryu[2]
[1]*Los Alamos National Laboratory, Los Alamos, New Mexico 87545, USA*
[2]*School of Mechanical Engineering, Chung-Ang University, Seoul, South Korea*

(Received 28 March 2018; published 6 September 2018)

We present a novel reaction analogy (RA) based forcing method for generating statistically stationary scalar fields in incompressible turbulence. The new method can produce more general scalar probability density functions (PDFs), for example, quasi-double-δ PDF, than current methods, while ensuring that scalar fields remain bounded, unlike existent forcing methodologies that can potentially violate naturally existing bounds. Such features are useful for generating initial fields in nonpremixed combustion, inlet conditions for spatially developing flows, or for studying non-Gaussian scalar turbulence. The RA method mathematically models hypothetical chemical reactions that convert reactants in a mixed state back into its pure unmixed components. Various types of chemical reactions are formulated and the corresponding mathematical expressions derived such that the reaction term is smooth in scalar space and is consistent with mass conservation. For large values of the scalar forcing rate, the method produces statistically stationary quasi-double-δ scalar PDFs. Quasiuniform, Gaussian, and stretched exponential scalar statistics are recovered for smaller values of the scalar forcing rate. The shape of the scalar PDF can be further controlled by changing the stoichiometric coefficients of the reaction. The ability of the new method to produce fully developed passive scalar fields with quasi-Gaussian PDFs is also investigated, by exploring the convergence of the scalar variance spectrum to the Obukhov-Corrsin scaling and of the third-order mixed structure function to the "four-thirds" Yaglom's law.

DOI: 10.1103/PhysRevFluids.3.094602

I. INTRODUCTION

Direct numerical simulations (DNS) that employ forcing mechanisms have provided insights into the nature of velocity [e.g., 1–15] and scalar field turbulence [e.g., 15–18] by maximizing the inertial range of scales simulated on a given mesh or focusing on the response of the flow when only certain scales are excited. Simulations with a forcing term can also be used to estimate the numerical dissipation in non-DNS codes as done in Ref. [19], by following a suggestion from Ref. [9]. In addition, statistically stationary turbulent fields have been employed as inflow conditions for numerical simulations of spatially developing flows [20,21].

In DNS studies of statistically stationary turbulence, various deterministic or random forcing terms usually mimic the energy supplied to the system by the natural shear production mechanism in the turbulent kinetic energy equation, $\langle \mathbf{u}' \cdot \nabla \langle \mathbf{u} \rangle \cdot \mathbf{u}' \rangle$, where $\mathbf{u}'$ represents the velocity fluctuations and $\nabla \langle \mathbf{u} \rangle$ is the mean velocity gradient. The velocity fluctuations can be replaced in this term with random noise or deterministic formulas, such that a specific form of the spectrum is obtained [16]. When the actual velocity fluctuations are used in the shear production term and $\nabla \langle \mathbf{u} \rangle$ is constant, the forcing term becomes linear in velocity [2,5,9]. Typically, isotropic turbulence simulations are

*livescu@lanl.gov

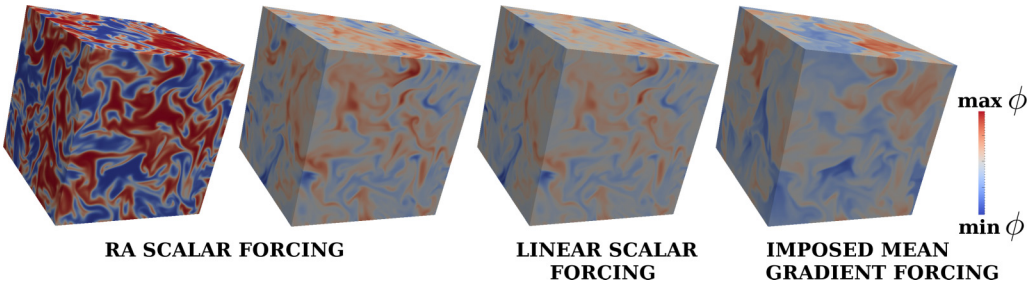

FIG. 1. Snapshots of the scalar field, ϕ, produced by the proposed RA (with different target scalar dissipation rates), LS, and IMG forcing methods. The underlying turbulent field is the same for all four cases.

forced only at low wave numbers. This maximizes the Reynolds number on a given mesh and ensures that the dynamics of the inertial range evolve naturally, without being influenced by the details of the forcing [22,23].

Scalar turbulence has been studied in the past by analogous linear forcing methods, for example by mimicking the natural production term in the scalar variance transport equation corresponding to a constant mean scalar gradient [16] (referenced to below as IMG) or direct analogy with the linear velocity forcing term [18] (referenced to below as LS). The former method produces anisotropic scalar fields due to the directionality imposed by the mean scalar gradient, while the latter produces isotropic scalar fields. Neither method though guarantees any bounds for the scalar field itself. While this may be relevant to some practical problems, there are many problems where the scalar quantities have natural bounds (e.g., mass or molar fractions vary between 0 and 1).

In addition, most studies to date of statistically stationary scalar turbulence concern Gaussian or quasi-Gaussian distributions, even though, generally, Gaussianity is not a common feature of scalar turbulence. Different types of scalar PDFs have been reported from laboratory experiments and numerical simulations of passive scalars, which include stretched exponentials [24–26], pure Gaussian, and sub-Gaussian PDFs [17,27]. Many practical problems naturally exhibit non-Gaussian scalar distributions, as is the case with multifluid flows such as scalar wakes, jets, or mixing layers, e.g., Refs. [28–30], buoyancy-driven turbulence [31–34], and nonpremixed combustion [35,36].

In this article, we propose a novel scalar forcing method based on a chemical reaction analogy (RA), which can produce more general scalar probability density functions (PDFs), for example quasi-double-δ PDF, compared to current forcing methods that are limited to producing Gaussian or near-Gaussian scalar PDFs. The new method also ensures the boundedness of the scalar field, in contrast to previous methods that can violate naturally existing bounds.

The RA method uses a hypothetical chemical reaction to convert the mixed fluid back into unmixed pure states. Reactants are identified based on a reaction analogy similar to that proposed in Ref. [33] to quantify the width of the Rayleigh-Taylor mixing layer and further generalized and discussed in Ref. [34]. Here, we consider even more general reaction rates together with their physical constraints to be used as forcing terms, and we discuss the resulting statistically stationary scalar fields and their dependence on the forcing term parameters. The resulting forcing term is nonlinear and has similarities with several well-studied reaction-diffusion systems, as well as the cubic Ginzburg-Landau equation. There are also some analogies with the description of certain reacting flows using the mixture fraction as a progress variable [37]. None of these equations has been used to generate turbulent stationary scalar fields, and, as far as we could find, the form of the forcing term presented here is new; nevertheless, such connections may be worth studying in the future.

To demonstrate the potential of the method, we illustrate the scalar fields produced by various scalar forcing methods in Fig. 1. The RA method can produce both large concentrations of pure states (red and blue) or mixed states (white). In contrast, LS and IMG forcings only produce a large amount of mixed states.

II. THEORY AND FORMULATIONS

We consider homogeneous isotropic turbulence governed by the incompressible constant density Navier-Stokes equations in a periodic box, subject to an explicit forcing term:

$$\nabla \cdot \boldsymbol{u} = 0, \quad \frac{\partial \boldsymbol{u}}{\partial t} + \boldsymbol{u} \cdot \nabla \boldsymbol{u} = -\nabla p + \nu \Delta \boldsymbol{u} + \boldsymbol{f}_{\boldsymbol{u}}, \tag{1}$$

where $\boldsymbol{u}$ is the (zero mean) velocity vector, p is the pressure normalized by the (constant) density and the forcing, $\boldsymbol{f}_{\boldsymbol{u}}$, supplies energy at a constant rate to wave numbers $k = \|\boldsymbol{k}\| < 1.5$. Maintaining a constant energy input rate has the advantage of being able to specify the Kolmogorov scale, η, and, thus, the degree at which the flow is resolved, at the onset [9].

The scalar field ϕ obeys an advection diffusion equation:

$$\frac{\partial \phi}{\partial t} + \boldsymbol{u} \cdot \nabla \phi = \mathcal{D} \nabla^2 \phi + \left[\underbrace{f(\boldsymbol{u})}_{\text{IMG}} \text{ or } \underbrace{f(\phi)}_{\text{LS or RA}} \right], \tag{2}$$

where f is the scalar forcing term. The kinematic viscosity, ν, and diffusion coefficient, $\mathcal{D}$, are constant.

Previous scalar forcings in Refs. [16] (denoted as IMG) and [15,18] (denoted as LS) are linear and consist of a coefficient multiplied with either a velocity component, u_i, or the scalar field, ϕ. The coefficient for the former is a constant mean scalar gradient while for the latter is instantaneously calculated to maintain a constant scalar variance.

The RA method mathematically models chemical reactions occurring between hypothetical reactants identified in a mixed fluid state. Consider a partially mixed fluid state, in which the number densities are such that there are N_A molecules of species A and N_B molecules of species B per unit volume. The molar masses of species A and B are identical and the total number of molecules per unit volume is assumed to be a constant, $N = N_A + N_B$, which is required by incompressibility. We define the molar fractions for species A, B as $X_A = N_A/N$, $X_B = N_B/N$. The scalar field ϕ can then be related to the molar fractions of species A and B. If $\phi \in [\phi_l, \phi_u]$, then $X_A = (\phi - \phi_l)/(\phi_u - \phi_l)$ and $X_B = (\phi_u - \phi)/(\phi_u - \phi_l)$, where ϕ_l and ϕ_u refer to the lower and upper bounds of the scalar field.

To formulate the reactions, we use ideas from a reaction analogy to describe mixing from Refs. [33,34]. Consider hypothetical chemical species, the mixed state reactant, M, and the excess state reactant, E. This can be either fluid A, i.e., E_A, or fluid B, i.e., E_B, depending if the mixture is either A or B rich. The mixed state M is defined to contain an equal number of A and B molecules, while the excess reactant can be either A or B, such that the total equals the local concentrations of A and B. In regions where $X_A < X_B$, the number of mixed state molecules (consisting of equal number of A and B molecules) per unit volume is $[M] = N_A$. The remaining molecules of B, i.e., $N - 2N_A$, are present in the excess state so that the number of excess state molecules per unit volume is $[E_B] = N - 2N_A = N_B - N_A$. Similarly, when $X_A > X_B$, we have $[M] = X_B$, $[E_A] = N_A - N_B$. Figure 2(a) illustrates the concentrations (or number densities) of M, E, A, and B as a function of ϕ.

A reaction between mixed and excess reactants can be represented by

$$\begin{aligned} mM + nE_B &\rightarrow (2m+n)E_B \quad \text{when } X_A \leqslant X_B, \\ mM + nE_A &\rightarrow (2m+n)E_A \quad \text{when } X_A > X_B, \end{aligned} \tag{3}$$

where m and n are the stoichiometric coefficients. These reactions constitute demixing processes that transform a partially mixed state into the excess pure component. In terms of the scalar field ϕ, the reactions transform the regions with below the average scalar values into the lower bound values and regions with above the average scalar values into the upper bound values. Thus, the reactions counteract the effect of diffusion.

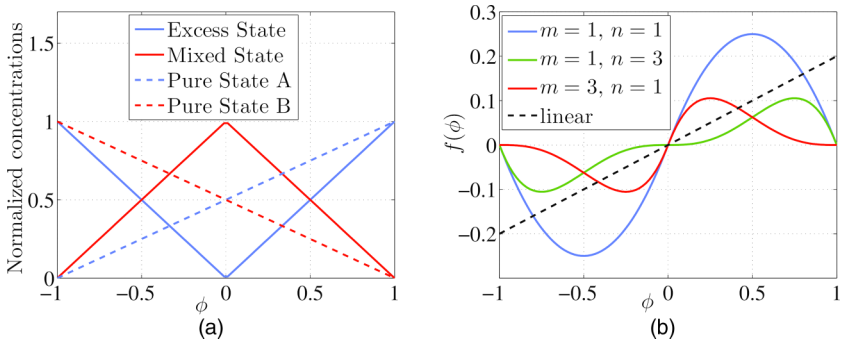

FIG. 2. RA forcing terms for different stoichiometric coefficients versus ϕ.

Using standard chemical kinetics formulas (e.g., Ref. [38]), the rate of increase of $[E_{B,A}]$ due to reactions Eqs. (3) between reactants M and $E_{B,A}$ is $2mK[M]^m[E_{B,A}]^n$, where K is the reaction rate constant. Expressing in terms of molar fractions, this becomes $2mKX_A^m(X_B - X_A)^n$ when $X_A < X_B$ and $2mKX_B^m(X_A - X_B)^n$ when $X_A > X_B$. In terms of the scalar field, the forcing term in $\dot{\phi}$ equation (after also transforming $\dot{E}_{B,A}$ into $\dot{\phi}$) further reduces to

$$f_\phi = \begin{cases} -(\phi_u - \phi_l)mK\left(\frac{\phi_u+\phi_l-2\phi}{\phi_u-\phi_l}\right)^n\left(\frac{\phi-\phi_l}{\phi_u-\phi_l}\right)^m; & \phi \leqslant \frac{\phi_u+\phi_l}{2} \\ (\phi_u - \phi_l)mK\left(\frac{2\phi-\phi_u-\phi_l}{\phi_u-\phi_l}\right)^n\left(\frac{\phi_u-\phi}{\phi_u-\phi_l}\right)^m; & \phi > \frac{\phi_u+\phi_l}{2}. \end{cases} \tag{4}$$

For simplicity, we choose the scalar bounds as $\phi_l = -1$ and $\phi_u = 1$. The forcing term can then be written in a compact form as

$$f_\phi = \text{sign}(\phi) f_c |\phi|^n (1 - |\phi|)^m, \tag{5}$$

where $f_c = 2mK/2^m$. Different choices of the stochiometric coefficients result in unique mathematical expressions for f_ϕ. For example, when $m = 3,\ n = 1$, the forcing acts less at large scalar magnitudes [Fig. 2(b)]. In comparison, linear forcing, also shown in Fig. 2(b), acts stronger at larger scalar magnitudes. Simpler reaction expressions of the type $A \to B,\ X_B > X_A$; $B \to A,\ X_A > X_B$ could also be devised; however, they are generally discontinuous at $\phi = 0$. Alternately, more complex reactions could be devised for example by changing the definition of the mixed state M.

There are several analogies between the forcing expression in Eq. (5) and well-known nonlinear reaction diffusion systems. For example, on each branch ($\phi < 0$ or $\phi > 0$) the $n = 1, m = 1$ formula is the same as Fisher's equation for spreading of advantageous allele within a given population [39]. Higher n, m values also lead to known equations on each branch, e.g., Newell-Whitehead-Segel equation describing Rayleigh-Benard convection or Zeldovich equation arising in combustion [39]. However, the reaction terms in these systems are not generally antisymmetric, which is a requirement for stationarity. For $n = 1$, $m = 2$, Eq. (5) reduces to $\phi(1 - |\phi|)^2$, which has some similarity with the reaction term in the cubic Ginzburg-Landau (GL) equation, $\phi(1 - |\phi|^2)$. The cubic GL equation arises naturally near critical phase transitions. If the linear term is positive (above the Hopf bifurcation, i.e., supercritical), the cubic term serves as a saturation to stop the growth of amplitude of the oscillations. If the linear term is negative (subcritical) and the cubic term is positive (excitation), the quintic term is needed to play the saturation role. The cubic GL equation is irreducible, so it is the simplest form that can describe such a bifurcation. There is also a parallel with combustion theory, in that an antisymmetric form of the reaction term can appear when the system is described by the mixture fraction as a progress variable for studying periodic reaction zones (e.g., Ref. [37]).

In summary, even though there are some similarities with several nonlinear reaction-diffusion systems, as far as we could find none of those systems has been used to generate stationary passive

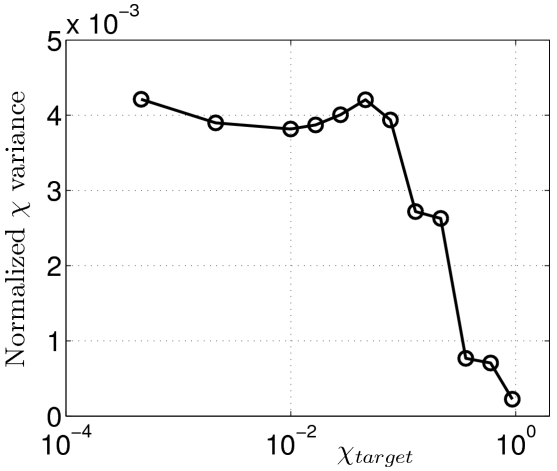

FIG. 3. The time variance over the stationary region of the volume averaged scalar dissipation normalized by χ^2 for different values of χ_{target}.

scalar turbulence with non-Gaussian PDFs and the particular form of our forcing term has not been studied before. Whether or not this form has practical relevance beyond our application could be an interesting topic, but it is outside the goals of our paper.

To eliminate the influence of small asymmetries in the initial scalar field, we further normalize the forcing expression. If this normalization is not performed, a particular reaction could be favored due to small numerical errors, transforming the entire scalar field into a trivial uniform state where either $\phi = -1$ (or ϕ_l in the general case) or $\phi = 1$ (or ϕ_u in the general case). To avoid this, the forcing is modified such that

$$f_\phi^* = \begin{cases} f_\phi / \| f_\phi \|_{\phi \in [-1,0]} & \text{when } \phi \leqslant 0 \\ f_\phi / \| f_\phi \|_{\phi \in (0,1]} & \text{when } \phi > 0. \end{cases} \tag{6}$$

At stationarity, after taking the time average, the scalar variance equation becomes

$$(-\chi + f_c \langle \phi f_\phi^* \rangle)_{\text{stationarity}} = 0, \tag{7}$$

where $\langle g \rangle$ represents the average (both over volume and time) of the quantity g and χ is the scalar dissipation, $\chi = \mathcal{D} \langle \nabla \phi \cdot \nabla \phi \rangle$. The stationary value of the dissipation can be chosen *a priori* by imposing the forcing coefficient to be

$$f_c = \frac{\chi_{\text{target}}}{\langle \phi f_\phi^* \rangle}, \tag{8}$$

where χ_{target} denotes the preselected scalar dissipation value at stationarity. The volume averaged scalar dissipation fluctuates around the target value and its time average is very close to χ_{target}. Indeed, the time variance of the volume averaged scalar dissipation displays very small values for all cases considered (Fig. 3). For the same velocity field and forcing parameters selected as described in Sec. III B, the IMG and LS methods produce scalar dissipation variances of 0.1 and 0.013, respectively, which are at least an order of magnitude larger than those shown in Fig. 3 for the RA method. In principle, these small dissipation fluctuations could be further reduced by considering a modification of the forcing term of the type proposed in Ref. [14] for velocity forcing. Since the variability of the scalar dissipation is relatively small, we have not explored such modification.

Selecting the value of the scalar dissipation at the onset, as done for the velocity field in Ref. [9] to control the resolution of the simulation (see below), can also be used to estimate the numerical

diffusion in non-DNS codes/simulations. Thus, at stationarity, relation Eq. (7) should still hold for non-DNS codes/simulations (e.g., in implicit large eddy simulations), with χ now being the sum of the numerical and physical (if any) scalar dissipations. Then f_c can be used to estimate the numerical scalar dissipation.

The numerical results are obtained with a spectral version of the CFDNS code [40], which follows a standard, fully dealiased pseudospectral algorithm using a combination of truncation and phase shifting, for incompressible Navier-Stokes equations with a passive scalar [29]. To demonstrate the method, all results presented correspond to a Schmidt number, $Sc = \nu/\mathcal{D} = 1$. The velocity field is linearly forced as described above following Refs. [5,9] and the target kinetic energy dissipation rate satisfies the resolution condition [9]

$$\epsilon_{\text{target}} = \frac{\nu^3}{(\eta k_{\max})_{\text{target}}} k_{\max}^4, \tag{9}$$

where $k_{\max} = \frac{\sqrt{2}}{3} N$ is the maximum resolved wave number for a grid size N^3, and η is the Kolmogorov microscale. $(\eta k_{\max})_{\text{target}}$ needs to be large enough for the solution to be well resolved on a given grid. This is fixed at either 1.5 or 3.0, as specified below. For simplicity, $\epsilon_{\text{target}} = 1.0$ for all cases. To maintain the required resolution, ν and $\mathcal{D}$ are changed appropriately to satisfy Eq. (9). Specifically, the simulations have been performed on 256^3, 512^3, and 1024^3 meshes, resulting in Taylor Reynolds numbers, Re_λ, ranging from 92 to 410. The turbulent kinetic energy at stationarity is $k_t = \langle \mathbf{u} \cdot \mathbf{u} \rangle / 2 \sim 3.0$. The results are averaged over 7, 3, and 1.5 eddy turnover times for the three mesh levels, respectively. During stationarity, both the instantaneous values of kinetic energy, $\epsilon = \nu \langle \boldsymbol{\nabla u} : \boldsymbol{\nabla u} \rangle$, and scalar, $\chi = \mathcal{D} \langle \boldsymbol{\nabla} \phi \cdot \boldsymbol{\nabla} \phi \rangle$, dissipation rates are close to their target values, ϵ_{target} and χ_{target}.

Most of the results below are obtained with stochiometric coefficients $m = 1$ and $n = 1$, unless otherwise indicated. To increase maximum allowable χ_{target}, the scalar bounds used in the forcing terms are smaller (i.e., $\{-0.98,\ 0.98\}$) than the actual scalar bounds, $\{-1,\ 1\}$.

III. RESULTS

In this section, we present some sample results to highlight the properties of the new forcing method. First, the influence of the forcing parameters and resolution on the resulting scalar PDF are discussed, followed by a comparison with IMG and LS forcings in terms of scalar bounds, variance, PDF, and mechanical to scalar dissipation timescale ratio. The spectral behavior of the terms in the scalar variance equation for low and high values of χ_{target} (or the forcing rate) is discussed next. Finally, we present results showing the convergence to the Obukhov-Corrsin spectral scaling for the scalar spectrum and to the 4/3 law for the mixed scalar-velocity third-order structure function.

A. The effects of forcing parameters on scalar PDF

We discuss the properties of the new RA forcing by examining how χ_{target} and the stoichiometric coefficients affect the scalar PDF, using 256^3 simulations, with $\eta k_{\max} = 3.0$ ($\Delta x \sim \eta$), corresponding to $\text{Re}_\lambda \sim 92$. This section also addresses the effect of resolution, using less resolved 256^3 simulations with $\eta k_{\max} = 1.5$ ($\Delta x \sim 2\eta$), and $\text{Re}_\lambda \sim 154$, as well as 512^3 and 1024^3 simulations with $\eta k_{\max} = 3.0$ and $\text{Re}_\lambda \sim 143$ and ~ 255, respectively.

Figure 4(a) illustrates the skewness, $S = -\frac{\langle \phi^3 \rangle}{\langle \phi^2 \rangle^{3/2}}$, and kurtosis, $K = \frac{\langle \phi^4 \rangle}{\langle \phi^2 \rangle^2}$, of the scalar PDFs generated by the RA forcing method for various target dissipation rates. Larger K values (i.e., more stretched PDFs) are produced for smaller χ_{target}, while S remains negligible for all χ_{target} values considered. Gaussian value of kurtosis is recovered by the method when $\chi_{\text{target}} \sim 0.01$. In terms of nondimensional quantities, this value corresponds to $\tau \sim 3.7$, where the scalar and energy turnover

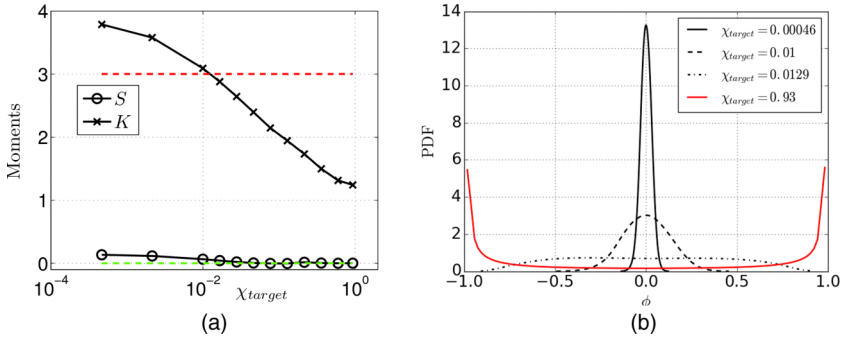

FIG. 4. (a) Skewness S (circles) and kurtosis (flatness) K (crosses) scalar PDF moments obtained for various target dissipation rates, χ_{target}, ranging from 0.00046 to 0.932. The Gaussian kurtosis of 3.0 is indicated with dashed lines. (b) Stationary scalar PDFs for different χ_{target} values.

timescale ratio is defined by

$$\tau = \frac{2k_t\,\chi}{\langle\phi^2\rangle\epsilon}. \tag{10}$$

Figure 4(b) shows the PDF profiles during the stationary period for four values of χ_{target}, 0.00046, 0.01, 0.129, and 0.932, corresponding to τ values of 3.2, 3.7, 4.2, and 8.4, respectively. As χ_{target} increases, the scalar field derivatives are larger, indicating the presence of more unmixed regions, with scalar values closer to the bounds. Thus, when $\chi_{\text{target}} = 0.00046$, the scalar PDF is more stretched than a Gaussian, with $K = 3.7$. $\chi_{\text{target}} = 0.01$ yields a stationary quasi-Gaussian PDF, while $\chi_{\text{target}} = 0.129$ results in a much flatter PDF (quasi-uniform), with $K = 1.9$. A further increase of χ_{target} to 0.932 produces a quasi-double-δ PDF with peaks near the forcing bounds and $K = 1.2$.

Figure 5(a) illustrates the scalar PDFs for the stochiometric coefficients $m = 1, 2, 3$ and $n = 1,\ 2,\ 3$, for $\epsilon_{\text{target}} = 0.01$. For $m = 1$, $n = 1$, the resulting scalar PDF is quasi-Gaussian, as explained above. When $m = 1$, $n = 2$, the PDF becomes a stretched exponential, with $K \sim 13$. The kurtosis continues to increase and reaches a value of ~30 for $m = 1$, $n = 3$. The results are consistent with the forcing term dependence on the scalar values shown in Fig. 2. Thus, as the coefficient n is increased, the forcing acts more on the rich A or B mixtures and less near the fully mixed fluid, allowing the existence of more partially mixed fluid. This results in more elongated tails in the scalar PDF. On the contrary, when the coefficient m is increased, Fig. 2 shows that the

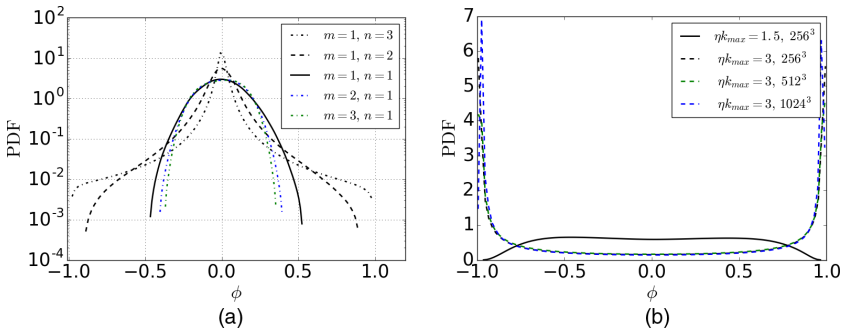

FIG. 5. (a) Effects of stochiometric coefficients on the scalar PDF with $\chi_{\text{target}} = 0.01$. (b) Scalar PDFs obtained for χ_{target} close to its largest χ_{target} value supported on a 256^3 mesh with $\eta k_{\text{max}} = 3.0$ ($\chi_{\text{target}} = 0.932$) and $\eta k_{\text{max}} = 1.5$ ($\chi_{\text{target}} = 0.17$). For comparison, scalar PDFs from 512^3 and 1024^3 simulations with $\chi_{\text{target}} = 0.932$ are also shown.

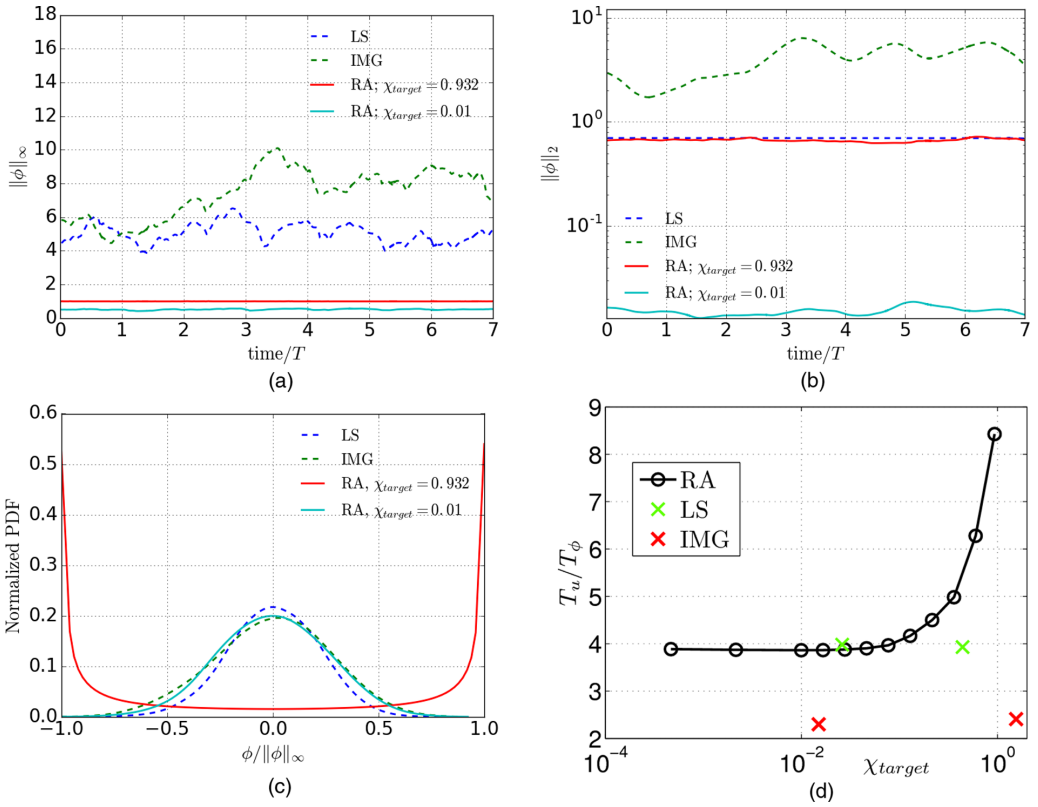

FIG. 6. (a) L_∞ norm and (b) L_2 norm of the scalar field using the RA, IMG, and LS methods. The x axis time is scaled with T, the eddy turnover time (~ 3.0) (c) Scalar PDFs produced by the RA, IMG and LS methods. (d) Mechanical to scalar dissipation timescale ratio comparison for the three forcing methods. The leftmost IMG and LS datapoints were obtained with mean scalar gradient of 0.1 and scalar variance matching the RA forcing with $\chi_{\text{target}} = 0.01$, respectively. The IMG and LS results are added to the plot based on their χ values.

forcing term acts stronger near the fully mixed fluid. This prevents the persistence of less mixed fluid, leaving a larger amount of fluid near the fully mixed value of $\phi = 0.0$. The resulting scalar PDFs have smaller kurtosis values, 2.4 and 2.3 for $m = 2,\ 3$, respectively [Fig. 5(a)].

For a given grid resolution, there is a maximum χ_{target} beyond which the scalar fields are ill-resolved, as the scalar gradients increase with χ_{target}. Conversely, for a fixed value of χ_{target}, as the resolution (i.e., ηk_{max}) decreases, at some point the scalar gradients can no longer be represented on the mesh. Figure 5(b) illustrates the scalar PDFs corresponding to a scalar dissipation rate close to its maximum allowable value on a 256^3 mesh, $\chi_{\text{target}} = 0.932$ for $\eta k_{\text{max}} = 3.0$ ($\Delta x \sim 2\eta$), and $\chi_{\text{target}} = 0.17$ for $\eta k_{\text{max}} = 1.5$ ($\Delta x \sim \eta$). The results show that a bimodal (quasi-double-δ) scalar PDF can only be obtained if the resolution is large enough to support the relatively large scalar gradients associated with this PDF. As the mesh size is increased, while maintaining $\eta k_{\text{max}} = 3.0$ and $\chi_{\text{target}} = 0.932$, the double-$\delta$ scalar PDF gets larger peaks.

B. Comparison with previous methods

The ability to produce statistically steady quasi double-delta scalar PDFs distinguishes the RA method from any previous methods such as IMG [16] or LS [18]. In addition, the RA method has ability to keep the scalar field within presscribed bounds. Figure 6(a) illustrates the temporal evolution of the L_∞ norm of the scalar field generated by RA with two χ_{target} values, IMG, and

LS methods. The simulations use identical velocity fields with $\mathrm{Re}_\lambda \sim 92$ and $\eta k_{\max} = 3.0$ on 256^3 meshes. The RA method uses $\chi_{\text{target}} = 0.01$, for a quasi-Gaussian scalar PDF and $\chi_{\text{target}} = 0.932$, which gives a quasi-double-δ scalar PDF. The mean scalar gradient used by the IMG method was chosen to be 1.0, while the forcing coefficient used by the LS method was chosen to match the scalar variance of the RA scalar with $\chi_{\text{target}} = 0.932$.

As Fig. 6(a) shows, the RA method keeps the scalar field within the specified bounds. For quasi-double-δ scalar PDF ($\chi_{\text{target}} = 0.932$), the scalar reaches its bounds, but the L_∞ scalar norm takes values slightly smaller than the prescribed bounds for $\chi_{\text{target}} = 0.01$, as the reaction is not fast enough compared to molecular diffusion to guarantee the presence of pure fluids. However, for the IMG and LS methods, the scalar can take much larger values. For these forcing methods, the scalar extrema become larger and larger by increasing the values of the forcing parameters such as the scalar variance, scalar dissipation rate, or the imposed mean scalar gradient.

There are no *a priori* analytical estimates for the scalar variance obtained through the IMG method, while LS forcing maintains a certain scalar variance value. This is reflected in the evolution of the L_2 norm shown in Fig. 6(b). The L_2 norm results for the RA method with quasi-double-δ PDF match the LS forcing results by design. As expected, for smaller values of χ_{target} with all other parameters fixed, the results indicate smaller stationary values for the scalar variance, as the scalar PDF starts peaking at $\phi = 0$.

Figure 6(c) compares the scalar PDFs obtained using the three methods. For $\chi_{\text{target}} = 0.01$, the RA and IMG results are close. By varying the mean scalar gradient for the IMG and forcing strength for the LS methods, the scalar PDF can depart slightly from a Gaussian (not shown), especially for the LS method where only certain parameters lead to a full Gaussian distribution, with a slightly stretched or compressed Gaussian being obtained in the general case.

The scalar dissipation rate is modeled in simpler mixing rate closures by assuming that the timescale ratio defined by Eq. (10) is constant [29,41]. For a passive scalar, the timescale ratio is typically about 2, although significant variations can exist depending on the flow conditions [16,29]. In combustion problems, τ can be an order of magnitude larger than 2 [41]. Figure 6(d) shows the timescale ratio obtained for the three forcing methods. For the range of parameters considered, the IMG method produces τ values close to 2, slightly increasing with the mean scalar gradient value. LS forcing results in τ values close to 4, while the timescale ratio for RA forcing varies depending on χ_{target}. For small χ_{target} values, $\tau \approx 4$, similar to LS forcing results, but takes much larger values as the scalar distribution becomes bimodal (e.g., $\tau \approx 8.4$ for $\chi_{\text{target}} = 0.932$). For homogeneous isotropic turbulence, the timescale ratio is proportional to the ratio of the scalar to velocity Taylor microscales [42]. As the scalar PDF becomes bimodal, the scalar variations are restricted to a thin diffusion layer separating the pure fluid regions. In this case, the scalar gradients become large, increasing the values of τ, offering a direct analogy with nonpremixed combustion problems.

C. Forcing spectrum

Since the RA forcing is nonlinear, it is interesting to see how the forcing spectrum varies with the wave number. To illustrate the importance of the forcing term at different wave numbers, we consider the spectral budget of the scalar variance transport equation:

$$\frac{\partial \langle \hat{\phi}\hat{\phi}^* \rangle}{\partial t} = \underbrace{\langle \hat{\phi}\hat{N}^* + \hat{\phi}^*\hat{N} \rangle}_{\text{Nonlinear transfer}} + \underbrace{\langle \hat{\phi}\hat{D}^* + \hat{\phi}^*\hat{D} \rangle}_{\text{Diffusion}} + \underbrace{\langle \hat{\phi}\hat{f}_\phi{}^* + \hat{\phi}^*\hat{f}_\phi \rangle}_{\text{Forcing}}, \tag{11}$$

where

$$N = -\boldsymbol{u} \cdot \nabla \phi, \tag{12}$$

$$D = \mathcal{D}\nabla^2 \phi. \tag{13}$$

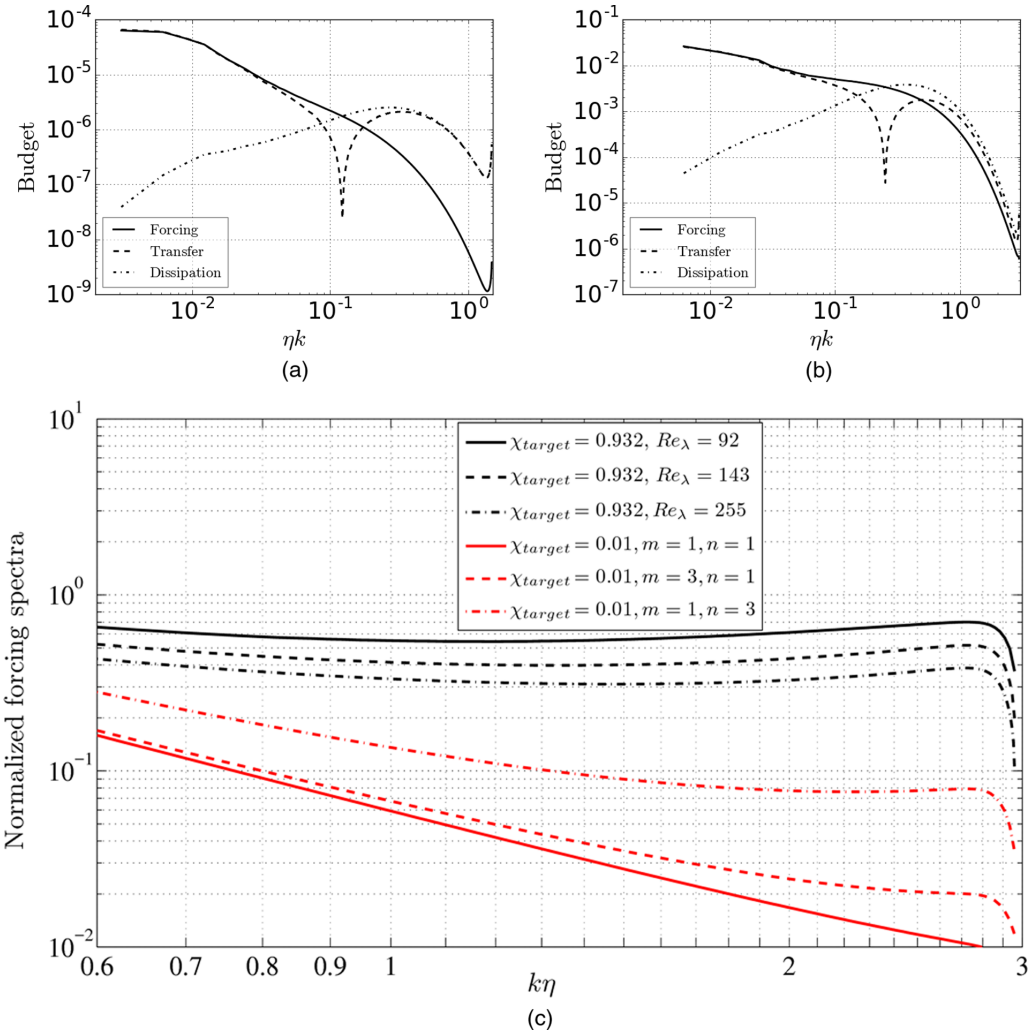

FIG. 7. Absolute values of the spectra of the terms contributing to spectral scalar variance equation. (a) $\chi_{\text{target}} = 0.01$, $\eta k_{\max} = 1.5$, $\text{Re}_\lambda = 410$, quasi-Gaussian scalar PDF, (b) $\chi_{\text{target}} = 0.932$, $\eta k_{\max} = 3$, $\text{Re}_\lambda = 255$, quasi-double-δ scalar PDF. (c) Forcing spectra normalized by the dissipation spectra in the dissipation range.

Here, the average, $\langle\rangle$, is over spherical shells and time (e.g., [43]),$\hat{}$ denotes the Fourier transform, and * is the complex conjugate. At stationarity, the time derivative on the left-hand side of Eq. (11) vanishes. Figure 7 shows the terms on the right-hand side of Eq. (11) from 1024^3 simulations with quasi-Gaussian ($\chi_{\text{target}} = 0.01$) and quasi-double-$\delta$ ($\chi_{\text{target}} = 0.932$) PDFs. At low χ_{target} values, RA forcing acts mostly at large scales, where it balances the transfer term, so that it leaves the small scalar scales largely unaffected [Fig. 7(a)]. However, for large values of χ_{target}, RA forcing can have a persistent influence at all wave numbers [Fig. 7(b)].

The forcing term does not contain spatial derivatives, so it is expected to decrease faster than the transfer and dissipation terms and to become negligible at high enough wave numbers. Indeed, that is the case with most of the RA forced simulations. For example, Fig. 7(c) shows that the forcing term increases in the dissipation range with the values of m and n, but remains more than an order of magnitude smaller than the dissipation term at small χ_{target} values. Even for the quasi-double-δ

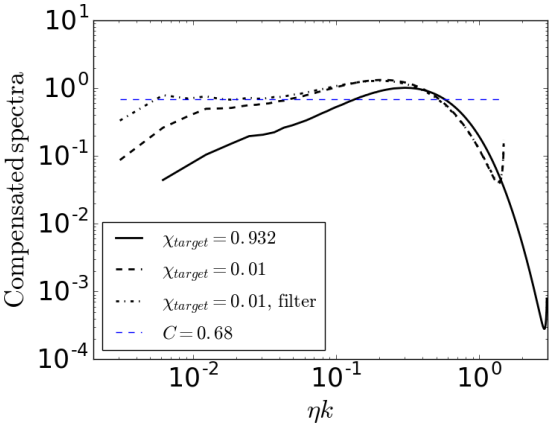

FIG. 8. Compensated scalar variance spectra, $\chi^{-1}\epsilon^{1/3}k^{5/3}E_{\phi}(k)$, versus the scaled wave number. Here, "filter" denotes a low wave number restriction of the RA forcing. The horizontal line corresponds to the Obukhov-Corrsin constant of 0.68.

PDF cases, which have the largest coefficient in front of the forcing term, that term is smaller than the dissipation term in the dissipation range. Due to the lack of spatial derivatives, it is possible to invoke locality arguments similar to Ref. [44] to show that for any forcing coefficient, there is a large enough Reynolds number for which the influence of the forcing term becomes negligible at small scales. This is consistent with results shown in Fig. 7(c) for quasi-double-δ scalar PDF ($\chi_{\text{target}} = 0.932$), which indicate that the forcing term importance at small scales decreases with increasing the Reynolds number. In the next section, we explore the ability of RA forced simulations to recover fully developed high Reynolds number passive scalar dynamics.

D. Recovering passive scalar dynamics

The idea of universality of statistical laws for turbulent fluctuations has been central for fundamental turbulence research for the past several decades. In general, numerical [4,12,43] and experimental [45] evidence indicates that the scaling exponents of the higher order scalar structure functions depend on the injection mechanism, i.e., temporal forcing for the former and initial conditions for the latter. Thus, scalar scaling satisfying the universal equilibrium theory, if practically realizable, may only be achieved under rather special circumstances. In practical applications, for example, in nonpremixed combustion, the non-Gaussian statistics of the scalar fields may significantly increase the intermittency and modify even more the scaling behavior.

Here, we first explore the ability of the RA forced simulations to produce fully developed scalar spectra. To obtain high Reynolds number scalar statistics with a finite mesh, one usually forces the scalar field only at low wave numbers to achieve a large separation of scales (e.g., Ref. [6,43]). Therefore, we have also performed a simulation corresponding to $\chi_{\text{target}} = 0.01$, where the RA forcing is restricted to $k \leqslant 1.5$. Figure 8 shows that the compensated scalar variance spectra develop a plateau at low wave numbers as a scale separation develops. The scalar spectrum and the Obukhov-Corrsin constant for the filtered RA forcing are very close to those obtained for similar Reynolds numbers using the low wave number scalar forcing in Ref. [43].

Next, we explore the ability of the RA forcing to recover the large Reynolds and Péclet numbers scaling of the mixed velocity scalar structure function (MSF). For stationary homogeneous isotropic velocity fields and homogeneous passive scalars, Yaglom's equation [43,46] for the MSF derivative reads

$$\frac{\partial\langle(\Delta_r\phi)^2\Delta_r u_r\rangle}{\partial \boldsymbol{r}} = -4\chi + 2\mathcal{D}\nabla_r^2\langle(\Delta_r\phi)^2\rangle + 2\langle\Delta_r\phi\Delta_r f_\phi\rangle. \tag{14}$$

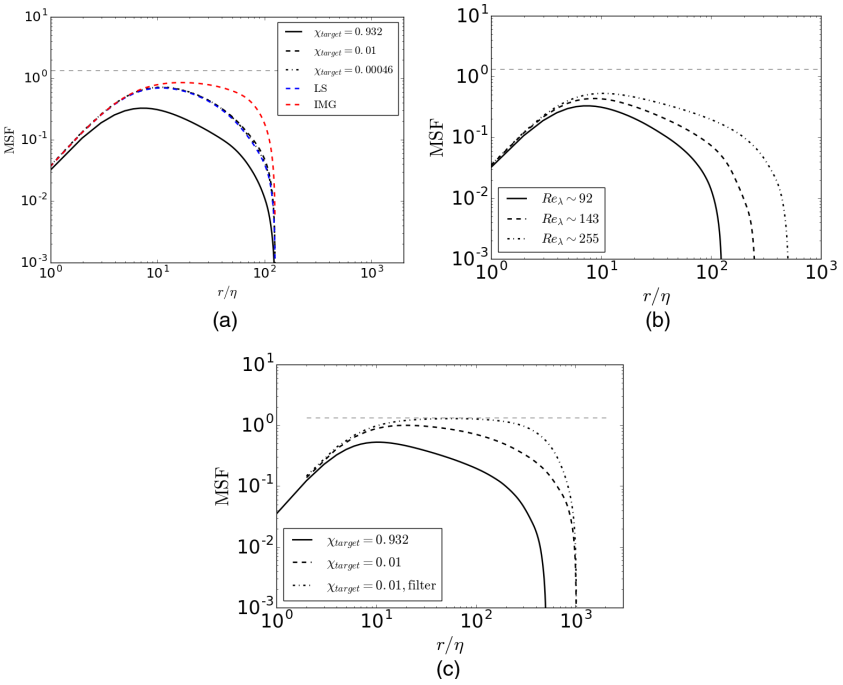

FIG. 9. MSF values for (a) $\mathrm{Re}_\lambda = 92$, with different forcing mechanisms; RA forcing corresponds to quasi-double-δ ($\chi_{\mathrm{target}} = 0.932$), quasi-Gaussian ($\chi_{\mathrm{target}} = 0.01$), and stretched ($\chi_{\mathrm{target}} = 0.00046$) scalar PDFs, (c) RA forcing for quasi-double-δ ($\chi_{\mathrm{target}} = 0.932$), $\mathrm{Re}_\lambda = 255$, and quasi-Gaussian ($\chi_{\mathrm{target}} = 0.01$), $\mathrm{Re}_\lambda = 410$, scalar PDFs. Here, "filter" denotes a low wave number restriction of the RA forcing.

The scalar, forcing, and longitudinal velocity differences between two spatial points separated by the displacement $\boldsymbol{r}$, with $r = \|\boldsymbol{r}\|$, are defined by $\Delta_r\phi = \phi(\boldsymbol{x}+\boldsymbol{r}) - \phi(\boldsymbol{x})$, $\Delta_r f_\phi = f_\phi(\boldsymbol{x}+\boldsymbol{r}) - f_\phi(\boldsymbol{x})$, and $\Delta_r u_r = (\boldsymbol{u}(\boldsymbol{x}+\boldsymbol{r}) - \boldsymbol{u}(\boldsymbol{x}))\cdot\boldsymbol{e_r}$, where $\boldsymbol{e_r}$ is a unit vector in the direction of displacement.

In regions much larger than Batchelor scale, η_B, the diffusion term becomes negligible. For scales much smaller than the energy containing scales, L, usually the forcing term contribution can also be neglected. After integrating over a ball of radius r, with $\eta_B \ll r \ll L$ [43], Yaglom's equation predicts [4,43,47,48]

$$-\frac{\langle(\Delta_r\phi)^2\Delta_r u_r\rangle}{\chi\, r} = \frac{4}{3}. \tag{15}$$

In general, when small χ_{target} values are imposed using the RA method, MSF values are very close and they are also close to LS forcing results and slightly below the IMG forcing results with parameters described in Sec. III B [Fig. 9(a)]. Simulations with larger values of χ_{target}, with quasi-double-δ scalar PDF as the limiting case, consistently yield lower MSF values at all Reynolds numbers examined. In this case, the prefactor is large enough to prevent the forcing term to vanish after integrating Yaglom's equation. Nevertheless, the justification given in Ref. [43] is still valid, so $\langle\Delta_r\phi\Delta_r f_\phi\rangle \to 0$ as $r \to 0$, and the forcing term contribution is expected to vanish at large enough Reynolds/Péclet numbers. Indeed, Fig. 9(a) shows that the MSF values become larger and seem to approach the 4/3 value as the Reynolds number is increased. However, full convergence to the 4/3 law may require much larger Re_λ values than those considered here. When the RA forcing is restricted to low wave numbers and the scalar PDF is quasi-Gaussian, Yaglom's law is fully recovered [Fig. 9(c)]. In this case, the results are consistent with previous forcing results using similar low wave number restrictions and Reynolds numbers [43]. In principle, one could minimize

the Reynolds number needed to reach fully developed scalar statistics with a quasi-double-δ PDF by using a combination of a low wave number restriction with a large χ_{target} value but such that the simulations are still well resolved. This could be the subject of a future study.

IV. CONCLUSIONS

We have presented a forcing method for producing stationary scalar fields in incompressible turbulence. The forcing term is constructed based on a hypothetical chemical reaction that transforms "mixed fluid" back into its "unmixed components" or "pure states." The reaction form is chosen to ensure that the forcing term satisfies mass conservation, is smooth in the scalar space, and unbiased with respect to the two pure states. By construction, the scalar fields stay within predefined bounds, unlike previous methods that can violate naturally existing bounds, while also allowing more general scalar PDFs than previous methods. This method can also be extended to variable density and fully compressible flows. While there are some similarities with several well-known nonlinear reaction-diffusion systems, as far as we could find none of those systems have been used to generate stationary passive scalar turbulence with non-Gaussian PDFs and the particular form of our forcing term has not been studied before. Whether or not this form has practical relevance beyond our application, for example in relation to the cubic Ginzburg-Landau equation, could be an interesting topic for future studies.

By varying the target scalar dissipation, which controls the strength of the forcing term, scalar PDFs can be changed to cover a large range of kurtosis values, from stretched exponential, to quasi-Gaussian, approximately flat, and quasi-double-δ PDF. Additional control on the shape of the scalar PDF can be exerted through the stoichiometric coefficients of the reactants (mixed and excess pure fluid) in the hypothetical reaction. As the χ_{target} value increases and the scalar PDF approaches a bimodal, quasi-double-δ shape, the timescale ratio of mechanical to scalar dissipation increases to large values, offering a direct analogy with nonpremixed combustion problems.

Since the forcing term does not contain spatial derivatives, it is expected to decrease at large wave numbers, compared to dissipation and nonlinear transfer terms in the spectral scalar variance equation. The results show that, while the forcing term increases at small scales with the stoichiometric coefficients (i.e., higher nonlinearities), for small values of the prefactor (i.e., χ_{target}), it remains much smaller than the dissipation term in the dissipation range. For large prefactor values, especially as a double-δ scalar PDF is approached, the forcing term (while still smaller than scalar dissipation) is no longer negligible in the dissipation range at $\text{Re}_\lambda = 92$. However, for all χ_{target} values, the forcing term decrease at small scales with increasing Re_λ, so presumably, fully developed scalar statistics with quasi-double-δ PDF can be obtained at large enough Reynolds numbers. When the forcing is restricted to low wave numbers, the compensated scalar variance spectra develop a plateau, with an Obukhov-Corrsin constant similar to previous studies with low wave number scalar forcing.

For all scalar PDFs, the third-order scalar-velocity structure function (MSF) increases as the Reynolds number is increased. Simulations with quasi-double-δ scalar PDF result in markedly lower MSF values than those with unimodal scalar PDFs. $\text{Re}_\lambda = 410$ results with quasi-Gaussian scalar PDF and scalar forcing restricted to small wave numbers fully recover Yaglom's $4/3$ scaling and are consistent with previous results with low wave number IMG forcing. The convergence to $4/3$ scaling is slower for simulations with large χ_{target} values, especially quasi-double-δ PDF, as the large prefactor of the forcing term requires much higher Reynolds number to achieve good separation of scales.

Previous studies indicate that scalar scaling following universal equilibrium theory may be obtained only under rather special circumstances, which may not be practically realizable. In many applications, scalar PDFs may be far from Gaussian (e.g., in nonpremixed combustion), which could significantly change the intermittency behavior and scaling of the scalar fields. While we have not explored such scalings here, we hope that the new tool we have introduced could start shedding some light on the fundamental properties of scalar mixing closer to practical applications.

ACKNOWLEDGMENTS

Los Alamos National Laboratory is operated by Los Alamos National Security, LLC for the U.S. Department of Energy NNSA under Contract No. DE-AC52-06NA25396. Computational resources were provided by the LANL Institutional Computing (IC) Program.

[1] K. Alvelius, Random forcing of three-dimensional homogeneous turbulence, Phys. Fluids **11**, 1880 (1999).
[2] T. S. Lundgren, Linearly forced isotropic turbulence, Annual Research Briefs, Center for Turbulence Research, Stanford University (2003), pp. 461–472, https://ctr.stanford.edu/annual-research-briefs-2003
[3] R. Rubinstein, T. T. Clark, D. Livescu, and L.-S. Luo, Time-dependent isotropic turbulence, J. Turbul. **5**, 11 (2004).
[4] T. Watanabe and T. Gotoh, Statistics of a passive scalar in homogeneous turbulence, New J. Phys. **6**, 40 (2004).
[5] C. Rosales and C. Meneveau, Linear forcing in numerical simulations of isotropic turbulence: Physical space implementations and convergence properties, Phys. Fluids **17**, 095106 (2005).
[6] P. K. Yeung, D. A. Donzis, and K. R. Sreenivasan, High-Reynolds-number simulation of turbulent mixing, Phys. Fluids **17**, 081703 (2005).
[7] T. Watanabe and T. Gotoh, Inertial-range intermittency and accuracy of direct numerical simulation for turbulence and passive scalar turbulence, J. Fluid Mech. **590**, 117 (2007).
[8] T. Ishihara, T. Gotoh, and Y. Kaneda, Study of high-Reynolds number isotropic turbulence by Direct Numerical Simulation, Annual Rev. Fluid Mech. **41**, 165 (2009).
[9] M. R. Petersen and D. Livescu, Forcing for statistically stationary compressible isotropic turbulence, Phys. Fluids **22**, 116101 (2010).
[10] P. C. Valente, R. Onishi, and C. B. da Silva, Origin of the imbalance between energy cascade and dissipation in turbulence, Phys. Rev. E **90**, 023003 (2014).
[11] S. Goto and J. C. Vassilicos, Energy dissipation and flux laws for unsteady turbulence, Phys. Lett. A **379**, 1144 (2015).
[12] T. Gotoh and T. Watanabe, Power and Nonpower Laws of Passive Scalar Moments Convected by Isotropic Turbulence, Phys. Rev. Lett. **115**, 114502 (2015).
[13] P. K. Yeung, X. M. Zhai, and K. R. Sreenivasan, Extreme events in computational turbulence, Proc. Natl. Acad. Sci. USA **112**, 12633 (2015).
[14] M. Bassenne, J. Urzay, G. I. Park, and P. Moin, Constant-energetics physical-space forcing methods for improved convergence to homogeneous-isotropic turbulence with application to particle-laden flows, Phys. Fluids **28**, 035114 (2016).
[15] J. A. Palmore and O. Desjardins, Technique for forcing high Reynolds number isotropic turbulence in physical space, Phys. Rev. Fluids **3**, 034605 (2018).
[16] M. R. Overholt and S. B. Pope, Direct numerical simulation of passive scalar with imposed mean gradient in isotropic turbulence, Phys. Fluids **8**, 3128 (1996).
[17] Z. Warhaft, Passive scalars in turbulent flows, Annual Rev. Fluid Mech. **32**, 203 (2000).
[18] S. Caroll, L. P. Verma, and G. Blanquart, A novel forcing technique to simulate turbulent mixing in a decaying scalar field, Phys. Fluids **25**, 095102 (2013).
[19] A. J. Wachtor, F. F. Grinstein, C. R. DeVore, J. R. Ristorcelli, and J. G. Margolin, Implicit large-eddy simulation of passive scalar mixing in statistically stationary isotropic turbulence, Phys. Fluids **25**, 025101 (2013).
[20] J. Ryu and D. Livescu, Turbulence structure behind the shock in canonical shock–vortical turbulence interaction, J. Fluid Mech. **756**, R1 (2014).
[21] D. Livescu and J. Ryu, Vorticity dynamics after the shock-turbulence interaction, Shock Waves **26**, 241 (2016).
[22] R. M. Kerr, Higher-order derivative correlations and the alignment of small-scale structures in isotropic numerical turbulence, J. Fluid Mech. **153**, 31 (1985).

[23] Y. Kaneda and T. Ishihara, High-resolution direct numerical simulation of turbulence, J. Turbul. **7**, N20 (2006).
[24] Jayesh and Z. Warhaft, Probability Distribution of a Passive Scalar in Grid-Generated Turbulence, Phys. Rev. Lett. **67**, 3503 (1991).
[25] F. A. Jaberi, R. S. Miller, C. K. Madnia, and P. Givi, Non-Gaussian scalar statistics in homogeneous turbulence, J. Fluid Mech. **313**, 241 (1996).
[26] B. I. Shraiman and E. D. Siggia, Scalar turbulence, Nature **405**, 639 (2010).
[27] M. Ferchichi and S. Tavoularis, Scalar probability density function and fine structure in uniformly sheared turbulence, J. Fluid Mech. **461**, 155 (2002).
[28] J. D. Li and R. W. Bilger, The diffusion of conserved and reactive scalars behind line sources in homogeneous turbulence, J. Fluid Mech. **318**, 339 (1996).
[29] D. Livescu, F. A. Jaberi, and C. K. Madnia, Passive scalar wake behind a line source in grid turbulence, J. Fluid Mech. **416**, 117 (2000).
[30] P. E. Dimotakis, The mixing transition in turbulent flows, J. Fluid Mech. **409**, 69 (2000).
[31] D. Livescu, Numerical simulations of two-fluid turbulent mixing at large density ratios and applications to the Rayleigh-Taylor instability, Phil. Trans. R. Soc. A **371**, 20120185 (2013).
[32] D. Chung and D. I. Pullin, Direct numerical simulation and large-eddy simulation of stationary buoyancy-driven turbulence, J. Fluid Mech. **643**, 279 (2010).
[33] A. W. Cook and P. E. Dimotakis, Transition stages of Rayleigh-Taylor instability between miscible fluids, J. Fluid Mech. **443**, 69 (2001).
[34] D. Livescu and J. R. Ristorcelli, Variable-density mixing in buoyancy-driven turbulence, J. Fluid Mech. **605**, 145 (2008).
[35] S. B. Pope, A rational method of determining probability distributions in turbulent reacting flows, J. Nonequil. Thermodynam. **4**, 309 (1979).
[36] A. G. Nouri, M. B. Nik, P. Givi, D. Livescu, and S. B. Pope, Self-contained filtered density function, Phys. Rev. Fluids **2**, 094603 (2017).
[37] M. R. Overholt and S. B. Pope, Direct numerical simulation of a statistically stationary, turbulent reacting flow, Combust. Theory Model. **3**, 371 (1999).
[38] F. A. Williams, *Combustion Theory* (Perseus Books, Cambridge, 1985).
[39] P. Grinrod, *The Theory and Applications of Reaction-Diffusion Equations: Patterns and Waves* (Clarendon Press, New York, 1996).
[40] D. Livescu, J. Mohd-Yusof, M. R. Petersen, and J. W. Grove, CFDNS: A Computer Code for Direct Numerical Simulation of Turbulent Flows, Tech. Rep. (Los Alamos National Laboratory, 2009) LA-CC-09-100.
[41] H. Kolla, J. W. Rogerson, N. Chakraborty, and N. Swaminathani, Scalar dissipation rate modeling and its validation, Combust. Sci. Tech. **181**, 518 (2009).
[42] C. Beguyer, I. Dekeyser, and B. E. Launder, Ratio of scalar and velocity dissipation timescales in shear flow turbulence, Phys. Fluids **21**, 307 (1978).
[43] T. Gotoh, T. Watanabe, and Y. Suzuki, Universality and anisotropy in passive scalar fluctuations in turbulence with uniform mean gradient, J. Turbul. **12**, N48 (2011).
[44] G. L. Eyink, Locality of turbulent cascades, Physica D **207**, 91 (2005).
[45] J. Lepore and L. Mydlarski, Effect of the Scalar Injection Mechanism on Passive Scalar Structure Functions in a Turbulent Flow, Phys. Rev. Lett. **103**, 034501 (2009).
[46] A. M. Yaglom, On the local structure of a temperature field in a turbulent flow, Dokl. Akad. Nauk SSSR **69**, 743 (1949).
[47] L. Danaila, F. Anselmet, T. Zhou, and R. A. Antonia, A generalization of Yaglom's equation which accounts for the large-scale forcing in heated decaying turbulence, J. Fluid Mech. **391**, 359 (1999).
[48] L. Danaila, R. A. Antonia, and P. Burattini, Comparison between kinetic energy and passive scalar energy transfer in locally homogeneous isotropic turbulence, Physica D **241**, 224 (2012).